Anisotropic wetting on tunable micro-wrinkled surfaces

Jun Young Chung,[a] Jeffrey P. Youngblood[b] and Christopher M. Stafford*[a]

Received 4th April 2007, Accepted 15th June 2007
First published as an Advance Article on the web 4th July 2007
DOI: 10.1039/b705112c

We examine the wettability of rough surfaces through a measurement approach that harnesses a wrinkling instability to produce model substrate topographies. Specifically, we probe the wetting of liquids on anisotropic micro-wrinkled features that exhibit well-defined aspect ratios (amplitude *versus* wavelength of the wrinkles) that can be actively tuned. Our study provides new insight into the wetting behavior on rough surfaces and into the interpretation of related liquid contact-angle measurements. In particular, we find that droplet wetting anisotropy is governed primarily by the roughness aspect ratio. In addition, comparison of our measurements to theoretical models demonstrates that droplet distortions and observed contact angles on surfaces with a strongly anisotropic texture can be quantitatively attributed to the difference in the energetic barriers to wetting along and perpendicular to substrate features.

Introduction

It is well known that liquid wetting on solids depends on both surface chemistry and physical factors such as surface roughness.[1–12] Quantitative understanding of this phenomenon underpins a huge range of technologies, including paints and coatings, biomaterials, microfluidics, and nanotechnology applications. The long history of scientific work examining effects of interfacial chemistry on wetting has benefited from the ability to fabricate model chemical surfaces for study, and such approaches have proliferated in recent years.[13] In contrast, measurements of the effect of surface roughness on wetting behavior suffer from the lack of model surfaces that systematically express key factors of surface topography (amplitude, spacing, anisotropy, *etc.*). In this paper, we exploit wrinkling phenomena[14] to produce well-defined topographies, and use these model surface textures to probe liquid-wetting behavior. Wrinkling is a fruitful testbed for studying wettability because the characteristic length scales of surface topography (*i.e.* wavelength and amplitude) can be systematically, precisely and actively tuned *via* simple changes in experimental conditions. Accordingly, our approach has significant advantages over routes that depend on more complex microfabrication. Moreover, our surface features exhibit a simple sinusoidal profile that is amenable to analysis by existing theoretical models. As discussed below, our study provides new observations and analysis of the wetting behavior of a liquid on surfaces with a strong anisotropic texture.[15,16]

[a]*Polymers Division, National Institute of Standards and Technology, 100 Bureau Drive, Gaithersburg, Maryland 20899, USA. E-mail: chris.stafford@nist.gov*
[b]*School of Materials Engineering, Purdue University, 501 Northwestern Avenue, West Lafayette, Indiana 47907, USA*

† Equipment and instruments or materials are identified in the paper in order to adequately specify the experimental details. Such identification does not imply recommendation by NIST, nor does it imply the materials are necessarily the best available for the purpose.

Experimental†

We fabricated anisotropic micro-wrinkled surfaces by mechanical compression of an ultraviolet–ozone (UVO)-treated poly(dimethylsiloxane) (PDMS) elastomer (see Fig. 1a).[17] The PDMS elastomer was prepared by mixing Sylgard 184 (Dow Chemical Co.) with a 10 : 1 ratio by mass of resin to curing agent, and curing at 75 °C for 2 h. The cross-linked PDMS film with a thickness of 1 mm was then cut into a rectangular shape (75 × 25 mm). A sheet of the cross-linked PDMS was initially mounted on a custom-designed strain stage,[18] and subsequently stretched uniaxially to a strain (ε) of 50%. The PDMS sheet was then exposed to UVO radiation (keeping a distance of ~7 mm between the sample and the light source) for an extended period of time (1 h), which oxidizes the outer surface of the PDMS sheet, converting it

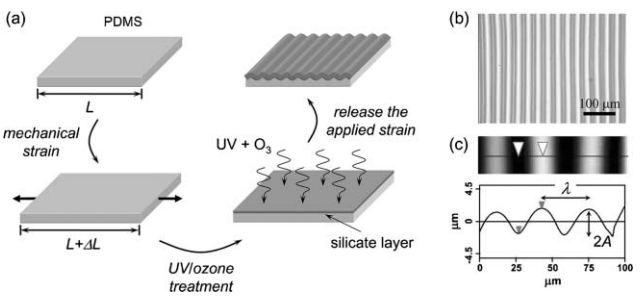

Fig. 1 (a) Schematic illustration of steps for generating sinusoidally micro-wrinkled patterns on PDMS substrates. A pristine poly(dimethylsiloxane) (PDMS) network is cast into thin (≈1 mm) films and subsequently stretched uniaxially up to 50%. The stretched substrate is then exposed to a UVO beam to produce the surface hydrophilic –OH groups. Finally, the strain is released from the modified PDMS substrate, causing the surface to form an undulating pattern. (b) Optical micrograph of wavy patterns on a PDMS substrate, as formed with a strain of 20% generated through mechanical compression. (c) Top view atomic force microscopy (AFM) image of the same sample and its corresponding surface height profile plotted along the line in black, showing a buckling wavelength (λ) of ≈32 μm and an amplitude (A) of ≈1.8 μm.

into a silicate-like layer. This layer can be separated into two distinct regions, namely, a dense silicate top layer of a few nanometres in thickness and a comparatively less dense intermediate layer of several tens of nanometres in thickness immediately underneath the dense layer. Note that the oxidation time for the UVO process alters both modulus of the oxidized layer as a function of depth beneath the surface and its thickness.[19] Upon releasing the strain from the pre-stretched UVO-PDMS substrate, a sinusoidally wrinkled pattern is generated perpendicular to the direction of the compressive strain. A typical optical micrograph of the parallel sinusoidal pattern and its topography, obtained *via* atomic force microscopy (AFM), are shown in Fig. 1b and 1c, respectively.

Surface wrinkling of this type is caused by the mismatch of elastic moduli between a relatively rigid surface layer and a more compliant elastomeric substrate.[14] Upon lateral compression of this system, periodic wrinkles are formed to minimize the strain energy above a certain threshold strain (ε_c). The characteristic periodicity (λ) of the wrinkling is determined by the mechanical properties of both the stiff film and the substrate:

$$\lambda = 2\pi h_f \left(\frac{\bar{E}_f}{3\bar{E}_s} \right)^{1/3}, \quad (1)$$

where $\bar{E} = E/(1 - \nu^2)$. E, h, and ν are the elastic modulus, the thickness and the Poisson's ratio for the film and substrate (f and s, respectively). The critical strain at which buckling occurs (ε_c) is a function of the ratio of elastic moduli:

$$\varepsilon_c = -\frac{1}{4} \left(\frac{3\bar{E}_s}{\bar{E}_f} \right)^{2/3}. \quad (2)$$

In addition, the amplitude of the buckling instability (A) depends on compressive strain as:

$$A = h_f \left(\frac{\varepsilon}{\varepsilon_c} - 1 \right)^{1/2}. \quad (3)$$

Combining the three equations above leads to the following expression for the roughness aspect ratio (A/λ) as:

$$\frac{A}{\lambda} = \frac{1}{\pi} (\Delta\varepsilon)^{1/2}, \quad (4)$$

where $\Delta\varepsilon = \varepsilon - \varepsilon_c$.

Based on eqn (1) and (3), the wrinkle wavelength is independent of compressive strain at small strains, which is known based on elastic post-buckling analysis, while the amplitude of the wrinkles is directly related to the strain. As the compressive strain increases, our experiments show that the wavelength does not change but the amplitude of wrinkling follows a square-root dependence with strain, as predicted by eqn (3) and previously verified experimentally.[17,20] Therefore, the wavelength and amplitude of the wrinkled surface can be controlled separately by adjusting UVO exposure dose and by manipulating the degree of compression, respectively. In addition, UVO-PDMS shows an excellent elastic recovery at least within the range of strains used in the present study ($\varepsilon \approx 40\%$). As a result, a precise and reversible control of patterned surface structure with a well-defined roughness aspect ratio becomes possible.[21] However, when UVO-PDMS substrates are compressed at relatively large strain (>40% in the present study), we observe a form of cracking along the strain direction (perpendicular to the wrinkled patterns). We believe that the origin of surface cracking is most likely due to the lateral deformation caused by Poisson's effect, which causes fracture of the silicate layer when the lateral deformation reaches its failure strain.

Contact-angle measurements were made by the sessile drop technique using a Krüss G2 contact-angle measuring system at ambient temperature. A deionized (DI) water droplet ($\approx$2 μL volume) was deposited on the sample surface and the static equilibrium contact angle (CA) was measured immediately upon needle removal. For each of the samples (smooth surface and wrinkled surfaces with different roughness aspect ratio), the static water CAs were measured in two directions: perpendicular ($\phi_\perp$) and parallel ($\phi_\parallel$) to the direction of the groove direction, as illustrated in Fig. 2b. The average of at least five measurements taken at different positions on each sample was used as the reported contact angle.

Results and discussion

Fig. 2a and 2b show aerial view microscope images of a water droplet on the smooth surface and the patterned surface, respectively. The unstrained UVO-PDMS surface is initially very smooth and the liquid–solid contact line (footprint) of the water droplet on the smooth surface is circular, as shown in Fig. 2a. A recent experiment by tapping-mode scanning force microscopy revealed that the PDMS-surface roughness does not change dramatically during UVO exposure.[22] However, the shape of the droplet on the micro-wrinkled surface is strongly influenced by geometrical anisotropy, and the contact line of a droplet placed on the patterned surface deviates from an ideal circle (Fig. 2b). As expected, this result shows that the anisotropy in surface topography plays a dominant role in developing anisotropic wetting behavior at the liquid–solid phase boundary. Fig. 2c and 2d show typical optical micrographs of a droplet of water on the structured surface in two close views (perpendicular and parallel). When the wetting direction (and contact-angle measurement) is *perpendicular* to the groove direction, the contact line of the droplet is shown to be straight and sticks to the peak of the sinusoidal groove (Fig. 2c). When adding or withdrawing water to and from the drop, we observe that the contact line advances or recedes in a stick-slip manner (the pinning–depinning–repinning transition along the groove peaks), suggesting that the source of this behavior is the energy barrier to movement of the contact line due to periodic sinusoid geometries. When the wetting direction is *parallel* to the grove direction, on the other hand, the droplet is elongated since there is no barrier to wetting along the path of groove, showing longer footage of the droplet compared to that in the perpendicular view. Interestingly, we see that the contact line is not smooth in the parallel direction but wavy across the geometric pattern (Fig. 2d). This local undulating pattern in the shape of the three-phase contact line closely resembles the sinusoidal surface pattern, showing a local pinning at the

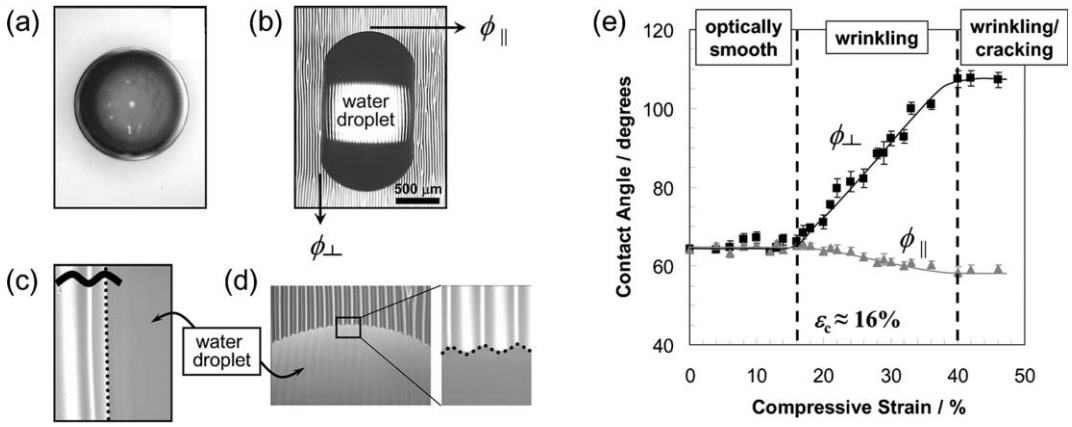

Fig. 2 (a) Top view optical micrograph of ≈2 μL water droplet on the smooth surface. (b)–(d) Optical micrographs of a water droplet on the patterned surface (ε = 30%), revealing an elongated, parallel-sided shape; (c) droplet showing evidence of pinning of contact line perpendicular to the grooves and (d) droplet spreading along the grooves. The arrows in (b) indicate the direction of contact-angle measurements. (e) Dependence of the water contact angles in two directions ($\phi_{\perp}$ and $\phi_{\parallel}$) on sinusoidally patterned surfaces as a function of degree of compression (ε). The lines are meant to guide the eye and the error bars represent one standard deviation of the data, which is taken as the experimental uncertainty of the measurement.

crest of the surface roughness and spreading at the bottom of the groove.

Surface wettability has predominantly been characterized by the contact angle, which is formed by a liquid at the three-phase (solid–liquid–air) boundary. We characterize the wetting properties more systematically by measuring the apparent contact angle (ϕ) on sinusoidally patterned surfaces as a function of compressive strain (*i.e.* different roughness aspect ratio). The results presented in Fig. 2e show the static water CAs measured perpendicular ($\phi_{\perp}$) and parallel ($\phi_{\parallel}$) to the direction of the grooves (the two configurations illustrated in Fig. 2b). Initially, the UVO-PDMS surface exhibits a mildly hydrophilic character with $\phi_{\perp} = \phi_{\parallel} = 64.3^{\circ} \pm 0.8^{\circ}$. As the compressive strain is raised stepwise from 0% (unstrained) to 50%, three distinct regimes are observed (see Fig. 2e): at low strains, CAs in both views ($\phi_{\perp}$ and $\phi_{\parallel}$) do not change until $\varepsilon \approx$ 16%, at which the wrinkling instability occurs (*i.e.* $\varepsilon_c \approx 16\%$; this result is fairly consistent with our observations *via* optical microscopy). As we increase the strain above 16%, $\phi_{\perp}$ starts to increase nearly linearly with increasing strain and then saturates at $\varepsilon \approx 40\%$ (square symbols in Fig. 2e). Conversely, $\phi_{\parallel}$ begins to decrease with increasing strain until $\varepsilon \approx 40\%$, and then plateaus for $\varepsilon > 40\%$ (triangle symbols in Fig. 2e). This observation can be explained by the fact that, at high strains (>40% in this case), UVO-modified PDMS shows signs of cracking parallel to the strain direction (Poisson's effect), which alters the initial hydrophilic nature of the UVO-PDMS surface. In the main discussion, we do not consider the CA data above $\varepsilon > 40\%$ since the cracking of the surface layer is known to promote transport of low molar mass molecules to the surface, resulting in hydrophobic recovery of the oxidized layer.[23,24]

In order to examine whether the increase in water CA with increasing surface roughness (in the case when $\varepsilon < 40\%$) shown in Fig. 2e is a result of hydrophobic recovery,[19,22–24] we carried out a systematic investigation on the changes in CA on the UVO-PDMS surfaces before and after the compressive strain (degree of compressive strain is fixed at 30%). Prior to compression, the surfaces show CA around 64° while, after compression, the equilibrium contact angles ($\phi_{\perp}$ and $\phi_{\parallel}$) exhibit the contact-angle anisotropy with higher values measured perpendicular to the grooves than those that are measured parallel to the groove direction, as shown before. $\phi_{\perp}$ increases up to a maximum near 92°, and $\phi_{\parallel}$ decreases to values close to 60° (see Fig. 3). When roughness is removed by stretching the sample back to its original shape (flat), the anisotropy becomes negligible and the contact angles approach the values for the smooth surface. The whole contact-angle transition is repeated over successive cycles by loading and unloading the elastic PDMS film, showing no noticeable increase in CA due to hydrophobic recovery. Such a reversible wettability change has recently aroused great interest, especially in reversible switching between superhydrophobicity and superhydrophilicity.[25] Although the observed reversibility of the wetting property reflects that hydrophobic recovery has a negligible effect, we observed that the hydrophobicity gradually increases with relatively long recovery time (at least two days), in agreement with Hillborg *et al.*[22] The hydrophobic recovery is believed to be a kinetically slow process. Thus, the effect of hydrophobic recovery should be negligible in terms of the enhanced hydrophobic transition on the patterned surface over the time scales (less than 1 h) of our experiments.

The results shown in Fig. 2 and 3 reveal the following features: (1) the difference in the wetting behavior in the two directions is attributed to the anisotropic and highly directional surface features; (2) the high contact angle measured as the contact line moves perpendicular across the grooves is due to pinning of the contact line whose motion exhibits periodic stick-slip behavior; (3) the low contact angle as the contact line moves parallel with the grooves is a result of preferential spreading of the droplet along the grooves due to roughness-enhanced wetting (Wenzel behavior[1]) as there exists no barriers to contact-line motion that would cause pinning. While adding water to the drop, the contact line undergoes continuous motion with a regular oscillatory wake; (4) although UVO-treated PDMS is inherently hydrophilic, the

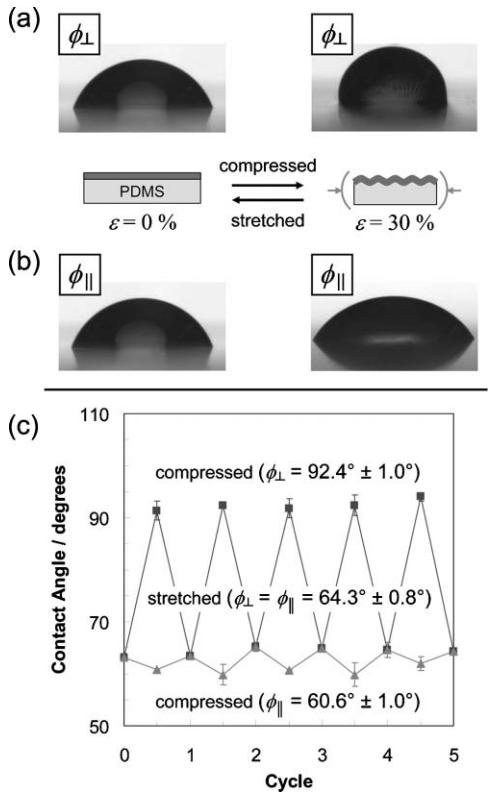

Fig. 3 (a)–(b) Images of water droplet shape in two views (perpendicular ($\phi_\perp$) and parallel ($\phi_\parallel$) to the direction of the grooves) on the surface before and after compression (ε = 30%). The wavelength (λ) and amplitude (A) of the wrinkles are ≈31 μm and ≈3.6 μm, respectively, which results in an aspect ratio (A/λ) of ≈0.11. (c) Changes in contact angles on the micro-wrinkled surface upon uniaxial compression and tension cycling, showing completely reversible wetting behavior. The error bars represent one standard deviation of the data, which is taken as the experimental uncertainty of the measurement.

anisotropic micro-wrinkled surface reported herein shows directionally dependant hydrophobicity, which is not due to hydrophobic recovery of the UVO-PDMS surface. This result implies that the change of contact angles on a real rough surface is significantly affected by the shape of the three-phase contact line.[5,9,26]

In order to better understand the above features, we perform an analysis on the basis of existing theoretical models. As a model for our experimental approach, we consider a liquid droplet placed on an idealized rough surface comprised of sinusoidal grooves of roughness factor (r), defined as the ratio of the true surface area to the projected surface area. We calculate the surface free energy as a function of the instantaneous contact angle along the same lines as those pioneered by Shuttleworth and Bailey[27] and later by Johnson and Dettre.[28] Johnson and Dettre[29] have also contrasted how a surface with symmetric concentric circles differs with symmetric parallel lines emanating from a central core. In the case of the latter geometry they explicitly state that the system would attain the angle of the global minimum free energy of the system. This work is instructive as to how we perform our calculations. In our case, we discretized the surface into two data sets handled independently: perpendicular and parallel. The perpendicular case is analogous to the concentric circular case of Johnson and Dettre and the parallel case is analogous to the symmetric parallel lines of Johnson and Dettre.

Fig. 4a depicts computer simulations of the free energy change in a perpendicular and parallel direction during the wetting of the structured surface with roughness factor 1.1 (the equivalent of ε = 30% in our experiments), respectively. A detailed description of how the data are simulated can be found in ref. 28. The smooth curve shown in Fig. 4a represents the free energy profile obtained for the direction along the grooves, exhibiting only a single minimum at 61.7°, which is slightly lower than the intrinsic CA (or Young's angle) on a smooth surface (64.3°). In the perpendicular direction, on the other hand, the free energy profile reveals the existence of multiple metastable configurations (undulating line in Fig. 4a). The envelope of the sinusoidal oscillatory curve corresponds to that of the smooth curve, which shares the same global energy minima, but with a number of metastable states centered around ϕ = 61.7°. In both cases, the global energy minimum is that which is predicted by the Wenzel model:[1]

$$\cos\phi = r(\cos\theta), \tag{5}$$

where r is Wenzel's roughness factor defined as the ratio of the true surface area to the projected surface area, and θ represents

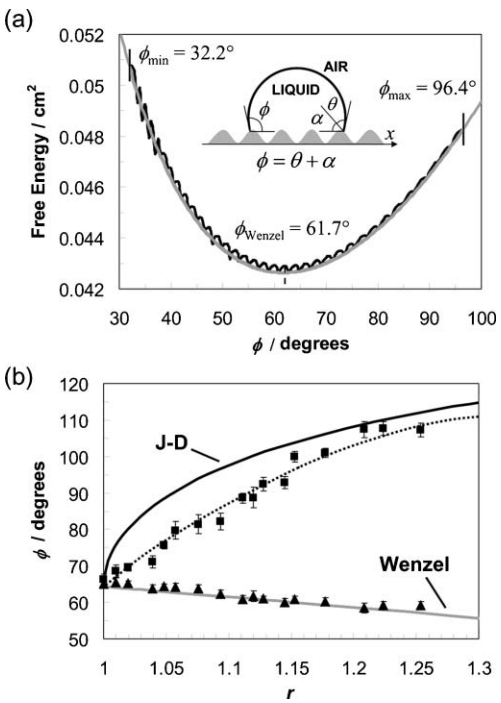

Fig. 4 (a) Free energy *versus* instantaneous contact angle for a water drop on a rough surface (Wenzel's roughness factor, $r \sim 1.1$; Young's angle on a smooth surface θ = 64.3°). The parallel and perpendicular directions for CA show one global minimum at 61.7° (smooth line) and the existence of numerous metastable states (undulating line), respectively. The vertical lines indicate the maximum and minimum possible contact angles. (b) Comparison of the experimental values ($\phi_\perp$ = square symbols; $\phi_\parallel$ = triangle symbols) with the calculated values (Wenzel model = lower line; Johnson and Dettre (J–D) model = upper line). The dotted line is meant to guide the eye.

the intrinsic contact angle. Eqn (5) demonstrates that a hydrophilic surface with surface features leads to a smaller contact angle due to a large geometric area for a relatively small projected area, increasing the energy of the surface due to the larger surface area. In the sinusoidal surface geometry, Wenzel's roughness factor is given by:[28]

$$r = \frac{4\pi A}{\lambda\rho^2}\int_0^{\rho}\left\{\frac{\lambda^2 x^2}{4\pi^2 A^2} + x^2\sin^2\frac{2\pi x}{\lambda}\right\}^{1/2} \mathrm{d}x, \qquad (6)$$

where ρ is the radius of the liquid drop on the surface. Based on this model using the same parameter values as given in the caption of Fig. 3, the Wenzel's angle of 61.7° can be predicted from eqn (5) and (6), which is in close agreement with the experimentally measured value (60.6° ± 1.0°). As shown in Fig. 2d, there is no obstacle for the drop to stick along the grooves in the case of wetting in the parallel direction. Thus, the metastable state should not exist and the system attains the most stable state – the global minimum – which corresponds to the value predicted by Wenzel. However, the observed CA perpendicular to the direction of grooves (92.4° ± 1.0°, see Fig. 3) is quite different from the equilibrium condition of 61.7° and deviates from the Wenzel equation mentioned above. This result can be understood by considering the potential barrier formed at the groove. When the wetting direction (and contact-angle measurement) is perpendicular to the groove, the energy barriers between adjacent grooves supposedly separates the existence of many metastable levels, and therefore the change in the free energy becomes discontinuous (stick-slip phenomenon). Although, as pointed out by Johnson and Dettre[30] and later by Marmur,[31] the system is always subject to some external disturbances (*e.g.* through vibrations in its environment), and this energy input may assist in overcoming energy barriers up to a certain level.

The anisotropic geometry also allows the liquid drop to preferentially spread along the groove rather than perpendicularly due to the higher energy required to overcome the energy barriers between metastable states, thus raising the contact angle necessary for contact-line motion. As the droplet is placed on the surface, the contact angle is increased until it approaches the angle necessary to advance the contact line. The contact line will advance when the lowest advancing contact angle along the periphery necessary for motion is attained – motion parallel to the grooves. As more water is added, contact line continuity eventually forces the angle in the perpendicular wetting direction to approach and attain the necessary angle for contact-line motion in that direction.

The correlations with the experimentally observed CAs on surfaces of controlled roughness are further investigated along the same line as in previously described models.[27,28] The schematic drawn in the inset of Fig. 4a illustrates a possible configuration of a liquid droplet, showing trapping into a metastable state near the crest of the groove. The observed macroscopic angle ϕ with respect to the horizontal is $\phi = \theta + \alpha$, where α is the angle of inclination of the surface at the point of liquid–solid contact, and θ is the microscopic local contact angle as required for energy minimization. For any given value of x, the inclination angle (α) is determined by $\alpha = \tan^{-1}[(2\pi A/\lambda)\sin(2\pi x/\lambda)]$. Since α is a maximum where $\sin(2\pi x/\lambda) = 1$ and a minimum where $\sin(2\pi x/\lambda) = -1$, the maximum and minimum inclinations of the surface, $\alpha_{max} = -\alpha_{min} = \tan^{-1}(2\pi A/\lambda)$. Based on the above geometrical argument, the maximum and minimum macroscopic angles are given by:[27,28]

$$\phi_{max} = \theta + \alpha_{max}, \qquad (7a)$$

$$\phi_{min} = \theta - \alpha_{max} \qquad (7b)$$

The vertical lines both at the beginning and end of the curve in Fig. 4a show the calculated values of $\phi_{max} = 96.4°$ and $\phi_{min} = 32.2°$ from eqn (7) using Wenzel's roughness factor, $r \sim 1.1$. These values represent absolute limits to advancing and receding contact angles based on geometry as calculated by Shuttleworth and Bailey[27] and are therefore, as Johnson and Dettre[28,30] noted, not likely to be observed as the barrier height may be zero at the periphery.

Fig. 4b shows experimental and theoretical CAs (predicted by Wenzel equation and eqn (7a)) *vs.* Wenzel's roughness factor (r) when Young's angle (θ) is 64.3°. Wenzel roughness factors were calculated for surfaces of different roughness from eqn (6) at the given values of A and λ. First, we show that all the measured CAs in the parallel direction (triangle symbols) agree well with the theoretical ones predicted by Wenzel equation (lower solid line). Second, the experimental CA measurements in the perpendicular view (square symbols) follow the general trend of the theoretical prediction obtained by eqn (7a) (upper solid line) and illustrate the effect of the anisotropic roughness on the CA increase. Comparison of these results suggests that the observed contact-angle anisotropy can be attributed solely to the roughness anisotropy. Furthermore, in view of the above experimental results, we may speculate that the reason why any system does not automatically assume Wenzel's configuration is that free energy barriers separate positions of metastable equilibrium. For a drop to remain in a position of metastable equilibrium, it is necessary that the external energy (*e.g.* vibration) of the drop be smaller than the height of the barrier beyond the metastable state of the contact line. For this reason, the actual values of the contact angles depend on the barrier heights and the vibrational state of the drop. It is important to realize that, as a first approximation, the energy barriers are proportional to the increasing ridge height (A) and ridge slope (α).[28,32] The lateral size of characteristic surface features (λ) also affects the height of the steps (energy barrier),[28,33] but does not influence the overall shape of the curve. Thus, the higher the aspect ratio of the roughness, the more difficult it is for the drop to overcome the physical barrier (the asperity). Therefore, the energy barriers between metastable states become higher and more difficult to overcome, resulting in a higher contact angle close to the theoretical maximum one; *i.e.* the experimental values approach the theoretical maximum contact-angle curve described by Shuttleworth and Bailey[27] as the roughness factor increases (see Fig. 4b).

Another issue is the effect of the Laplace pressure on the wetting of the fluid on the surface. The Laplace pressure is related to the size of the pore and the equilibrium surface energy of the pore in relation to the penetrating liquid. For a

wetting liquid, which is the case here, the liquid should fully penetrate the pores and the system should stay fully in the Wenzel regime. In the case of contact-line motion parallel to the roughness, there is no issue. However, in the perpendicular case there exists a problem where the advancing contact angle is high enough so that the Laplace equation dictates that the fluid should not penetrate the grooves. It is our argument that the contact line will pin at the highest energy barrier (near the tops) until the advancing drop forces the contact line past this sticking point and the lower surface energies again dominate allowing fluid penetration. In other words, in this case, there is a decoupling between the observed contact angle and the wetting of the fluid on the surface.

In the present study, we observed that the condition θ (intrinsic contact angle) $>90^\circ$ does not constitute a real limitation towards obtaining high contact angles, and hydrophobic surfaces can be obtained even when the thermodynamic contact angle θ is smaller than 90°, although such configurations are metastable (related works were reported in the literature[34]). On the other hand, contact-angle values approaching ϕ_{max} and ϕ_{min} are not likely to be observed in a hydrophilic isotropic structure, in which the contact angle decreases as a result of the surface roughness. In this situation, any barrier to contact-line motion in which the surface would act as our perpendicular case can be circumvented by pathways around the barrier where the surface would act as our parallel case and attain the global minimum. Thus, the apparent contact angle can be usually modeled by either Wenzel's[1] or Cassie–Baxter's theory,[2] depending on how a liquid droplet is formed. This result has been analyzed recently by Carbone and Mangialardi[35] who considered the liquid drop lying on a simple sinusoidal profile, as used in the current study.

Conclusions

This study shows promising prospects for the buckling-based technique in the fabrication of tunable wrinkled microstructures. We show that a liquid droplet on surfaces with geometrically anisotropic patterns shows anomalous wetting behavior, which is in contrast to droplets on isotropically patterned surfaces. The relationship between the micro-wrinkled surfaces and the anisotropic wetting has been discussed on the basis of the comparison of the experimental values with theoretical ones obtained from both the Wenzel model and Johnson and Dettre model. An increase in pinning barriers due to increase in the height of the sinusoidal grooves is believed to be responsible for the amplification of the contact angle measured perpendicular to the direction of the wrinkles. Our account of the anisotropic wetting implies that the change of contact angles on a real rough surface is significantly affected by the nature of the three-phase contact-line structure, rather than by simply increasing surface roughness. These findings not only provide insight into the wetting behavior on a rough surface but also open up another potential door for a number of applications that require directional and spatial variations of physical properties, such as controlled wetting, adhesion and friction.

Acknowledgements

The authors thank Michael J. Fasolka for critically reading the manuscript and Joong Tark Han and Vijay R. Tirumala for insightful discussions. This work was conducted at the NIST Combinatorial Methods Center. This manuscript is an official contribution of the National Institute of Standards and Technology; not subject to copyright in the United States.

References

1 R. N. Wenzel, *Ind. Eng. Chem.*, 1936, **28**, 988–994.
2 A. B. D. Cassie and S. Baxter, *Trans. Faraday Soc.*, 1944, **40**, 546–551.
3 E. G. Shafrin and W. A. Zisman, *Adv. Chem. Ser.*, 1964, **43**, 145–157.
4 J. Bico, C. Marzolin and D. Quéré, *Europhys. Lett.*, 1999, **47**, 220–226.
5 D. Öner and T. J. McCarthy, *Langmuir*, 2000, **16**, 7777–7782.
6 A. Lafuma and D. Quéré, *Nat. Mater.*, 2003, **2**, 457–460.
7 N. A. Patankar, *Langmuir*, 2003, **19**, 1249–1253.
8 C. W. Extrand, *Langmuir*, 2003, **19**, 3793–3796.
9 C. W. Extrand, *Langmuir*, 2005, **21**, 10370–10374.
10 M. Callies and D. Quéré, *Soft Matter*, 2005, **1**, 55–61.
11 X. Feng and L. Jiang, *Adv. Mater.*, 2006, **18**, 3063–3078.
12 L. Gao and T. J. McCarthy, *Langmuir*, 2007, **23**, 3762–3765.
13 M. K. Chaudhury and G. M. Whitesides, *Science*, 1992, **256**, 1539–1541; J. Genzer and K. Efimenko, *Science*, 2000, **290**, 2130–2133; T. P. Russell, *Science*, 2002, **297**, 964–967; S. Khongtong and G. S. Ferguson, *J. Am. Chem. Soc.*, 2002, **124**, 7254–7255; D. Julthongpiput, M. J. Fasolka, W. H. Zhang, T. Nguyen and E. J. Amis, *Nano Lett.*, 2005, **5**, 1535–1540.
14 H. G. Allen, *Analysis and Design of Structural Sandwich Panels*, Pergamon Press, Oxford, 1969; N. Bowden, S. Brittain, A. G. Evans, J. W. Hutchinson and G. M. Whitesides, *Nature*, 1998, **393**, 146–149; A. L. Volynskii, S. Bazhenov, O. V. Lebedeva and N. F. Bakeev, *J. Mater. Sci.*, 2000, **35**, 547–554; J. Groenewold, *Physica A*, 2001, **298**, 32–45; J. Genzer and J. Groenewold, *Soft Matter*, 2006, **2**, 310–323; E. P. Chan and A. J. Crosby, *Soft Matter*, 2006, **2**, 324–328.
15 For related articles on the anisotropic wetting of rough surfaces, see: R. J. Good, J. A. Kvikstad and W. O. Bailey, *J. Colloid Interface Sci.*, 1971, **35**, 314–327; Z. Yoshimitsu, A. Nakajima, T. Watanabe and K. Hashimoto, *Langmuir*, 2002, **18**, 5818–5822; Y. Chen, B. He, J. Lee and N. A. Patankar, *J. Colloid Interface Sci.*, 2005, **281**, 458–464; A. D. Sommers and A. M. Jacobi, *J. Micromech. Microeng.*, 2006, **16**, 1571–1578; Y. Zheng, X. Gao and L. Jiang, *Soft Matter*, 2007, **3**, 178–182; Y. Zhao, Q. Lu, M. Li and X. Li, *Langmuir*, 2007, **23**, 6212–6217.
16 For related articles on the anisotropic wetting of chemically-structured surfaces, see: A. Marmur, *J. Colloid Interface Sci.*, 1994, **168**, 40–46; H. Gau, S. Herminghaus, P. Lenz and R. Lipowsky, *Science*, 1999, **283**, 46–49; M. Gleiche, L. Chi, E. Gedig and H. Fuchs, *ChemPhysChem*, 2001, **3**, 187–191; M. Morita, T. Koga, H. Otsuka and A. Takahara, *Langmuir*, 2005, **21**, 911–918.
17 K. Efimenko, M. Rackaitis, E. Manias, A. Vaziri, L. Mahadevan and J. Genzer, *Nat. Mater.*, 2005, **4**, 293–297.
18 C. M. Stafford, C. Harrison, K. L. Beers, A. Karim, E. J. Amis, M. R. Vanlandingham, H.-C. Kim, W. Volksen, R. D. Miller and E. E. Simonyl, *Nat. Mater.*, 2004, **3**, 545–550; C. M. Stafford, S. Guo, C. Harrison and M. Y. M. Chiang, *Rev. Sci. Instrum.*, 2005, **76**, 062207-1–062207-5.
19 M. Ouyang, C. Yuan, R. J. Muisener, A. Boulares and J. T. Koberstein, *Chem. Mater.*, 2000, **12**, 1591–1596; K. Efimenko, W. E. Wallace and J. Genzer, *J. Colloid Interface Sci.*, 2002, **254**, 306–315; A. Olàh, H. Hillborg and G. J. Vancso, *Appl. Surf. Sci.*, 2005, **239**, 410–423.
20 C. Harrison, C. M. Stafford, W. Zhang and A. Karim, *Appl. Phys. Lett.*, 2004, **85**, 4016–4018.
21 For example, the surface height profile in Fig. 1c shows a buckling wavelength (λ) of $\approx$32 μm and an amplitude (A) of $\approx$1.8 μm, resulting in an aspect ratio (A/λ) of $\approx$0.056 (when ε = 20%). This aspect ratio of roughness coincides well with the theoretical value

(≈0.063) obtained from eqn (4), setting $\varepsilon_c \approx 16\%$ (which is determined by optical microscope images as well as contact-angle measurements; also see Fig. 2e). This result indicates that buckling-based technique can be easily utilized to obtain the precise surface-feature patterning.
22 H. Hillborg, N. Tomczak, A. Olàh, H. Schönherr and G. J. Vancso, *Langmuir*, 2004, **20**, 785–794.
23 J. Kim, M. K. Chaudhury and M. J. Owen, *IEEE Trans. Dielectr. Electr. Insul.*, 1999, **6**, 695–702; J. Kim, M. K. Chaudhury and M. J. Owen, *J. Colloid Interface Sci.*, 2000, **226**, 231–236.
24 H. Hillborg and U. W. Gedde, *IEEE Trans. Dielectr. Electr. Insul.*, 1999, **6**, 703–717.
25 J. Zhang, X. Lu, W. Huang and Y. Han, *Macromol. Rapid Commun.*, 2005, **26**, 477–480; X. Yu, Z. Wang, Y. Jiang, F. Shi and X. Zhang, *Adv. Mater.*, 2005, **17**, 1289–1293; F. Xia, L. Feng, S. Wang, T. Sun, W. Song, W. Jiang and L. Jiang, *Adv. Mater.*, 2006, **18**, 432–436; J. T. Han, S. Kim and A. Karim, *Langmuir*, 2007, **23**, 2608–2614.
26 W. Chen, A. Y. Fadeev, M. C. Hsieh, D. Öner, J. P. Youngblood and T. J. McCarthy, *Langmuir*, 1999, **15**, 3395–3399.
27 R. Shuttleworth and G. L. J. Bailey, *Discuss. Faraday Soc.*, 1948, **3**, 16–22.
28 R. E. Johnson, Jr. and R. H. Dettre, *Adv. Chem. Ser.*, 1964, **43**, 112–135.
29 R. E. Johnson, Jr. and R. H. Dettre, *J. Phys. Chem.*, 1964, **68**, 1744–1750.
30 R. E. Johnson, Jr. and R. H. Dettre, in *Surface and Colloid Science*, ed. E. Matijevic, Wiley-Interscience, New York, 1969, vol. 2, pp. 85–153.
31 A. Marmur, *Soft Matter*, 2006, **2**, 12–17.
32 J. D. Eich, R. J. Good and A. W. Neumann, *J. Colloid Interface Sci.*, 1975, **53**, 235–238.
33 J. P. Youngblood, Ph.D. Thesis, University of Massachusetts Amherst, 2001.
34 S. Herminghaus, *Europhys. Lett.*, 2000, **52**, 165–170; L. Feng, Y. Song, J. Zhai, B. Liu, J. Xu, L. Jiang and D. Zhu, *Angew. Chem., Int. Ed.*, 2003, **42**, 800–802; Q. Xie, G. Fan, N. Zhao, X. Guo, J. Xu, J. Dong, L. Zhang, Y. Zhang and C. C. Han, *Adv. Mater.*, 2004, **16**, 1830–1833; M. E. Abdelsalam, P. N. Bartlett, T. Kelf and J. Baumberg, *Langmuir*, 2005, **21**, 1753–1757.
35 G. Carbone and L. Mangialardi, *Eur. Phys. J. E*, 2005, **16**, 67–76.